CONF-781033--2

MASTER

LA-UR -78-2957

TITLE: A REVIEW OF THE PHYSICAL PROPERTIES OF LIQUID IONIZATION CHAMBER MEDIA

AUTHOR(S): Charles R. Gruhn
Robert Loveman

SUBMITTED TO: 1978 IEEE Nuclear Science Symposium
Washington, DC
October 18-20, 1978

los alamos
scientific laboratory
of the University of California
LOS ALAMOS, NEW MEXICO 87545

An Affirmative Action/Equal Opportunity Employer

Form No. 836 R2
St. No. 2629
1/78

DEPARTMENT OF ENERGY
CONTRACT W-7405-ENG. 36

A REVIEW OF THE PHYSICAL PROPERITIES OF LIQUID IONIZATION CHAMBER MEDIA*

Charles R. Gruhn+ and Robert Lovemant

Abstract

We review those physical properties of liquid methane, argon, krypton, and xenon important in the design, construction, and operation of liquid ionization chambers. The thermodynamic properties, electrical and optical properties, effects of impurities, and atomic and nuclear properties are summarized.

I. Introduction

In this review we present a collection of representative data pertaining to the physical properties of liquid methane, argon, krypton, and xenon, which we believe will be useful in the design, construction, and operation of liquid ionization chambers. Wherever possible we shall also present sufficient theoretical guidance to allow either interpolation or extrapolation of the data. We do not attempt to exhaustively review any one specific physical property of the liquids but rather refer the reader to the literature where this has been done.

We divide our review into four sections: Thermodynamic Properties, Electrical and Optical Properties, Effect of Impurities, and Atomic and Nuclear Properties. Two excellent reviews on the thermodynamic properties by R. K. Crawford[1] and by A. C. Hollis Hallett[2] have been published and are used extensively in this paper. In the Electrical and Optical Properties section and Impurities section, the reviews relating to electron scavenging and free carrier yields by A. Hummel[3] and A. Mozumder[4] are used. The remainder of the material presented has been screened arbitrarily from the literature and is referenced.

2. Thermodynamic Properties

2.1 Principle of Corresponding States

The principle of corresponding states[1,5-8] says that there exists universal relationships describing the phase boundaries and equations of states when the temperature, pressure, and density are expressed in suitably reduced units. Generally these reduced units are given in terms of either the triple point or critical point constants. A statistical development of the principle of corresponding states is given by Boer and Michels,[5] K. Pitzer,[6] and E. A. Guggenheim.[7] A recent examination of the principle of corresponding states and liquid argon, krypton, and xenon is given by W. B. Streett and L. A. K. Staveley.[8] Our reason for introducing the principle here is that it provides an excellent basis for the interpolation and extrapolation of the thermodynamic properties. Deviations from the corresponding states principle are usually associated with quantum mechanical differences in the excitation of internal degrees of freedom. These deviations are quite small for argon, krypton, and xenon and are somewhat larger as one would expect for methane.

+University of California
Los Alamos Scientific Laboratory
Los Alamos, New Mexico 87545

†University of Washington
Seattle, Washington 98195

In Table I we list some of the triple and critical point properties of methane,[9] argon,[1] krypton,[1] and xenon.[1] The errors in the properties given are in the last digit. A more complete description of the errors are given in the references.[1,9] The ratio of the triple point to critical point properties are essentially constant for the rare gases ($T_t/T_c = 0.555$, $P_t/P_c = 0.14$, $\rho_t/\rho_c = 2.66$) with methane deviating slightly. The entropy changes upon evaporation $L_v/T_t = 18.9 \frac{cal}{mole\ K}$, $L_c/T_t = 3.40 \frac{cal}{mole\ K}$ are also nearly the same for the rare gases.

2.2 Phase Diagram and Equations of State

Applying the principle of corresponding states to methane, argon, krypton, xenon, we find that the phase diagrams are the same to within a few precent. In Fig. 1 we show the phase diagram for these gases.

The vaporation curves can be fitted to a simple expression applying the principle of corresponding states.

$$\ln(P/P_c) = A(1 - T_c/T \qquad (1)$$

We choose to fit this expression at the triple point. The values of the one free parameter, A, are given in Table II. The pressures as a function of temperature are accurate to about one percent and are precise at the triple and critical points. A more precise expression[10] (.1%) is fitted to data involving 16 to 17 parameters.[11,12]

The melting curve is given by the Simon equation,[13] which is reviewed extensively by S. E. Babb, Jr.[14] for numerous materials.

$$(P/P_t - 1) = B\,(T/T_t)^c - 1 \qquad (2)$$

The two free parameters, B and c, are listed in Table II. The near equality of these parameters for the rare gases reflects the validity of the principle of corresponding states.

The temperature dependence of the density of the liquid is given by the Guggenheim[7] expression to within two percent.[9]

$$\rho_l/\rho_c = 1 + \frac{3}{4}(1 - T/T_c) + \frac{7}{4}(1 - T/T_c)^{\frac{1}{3}} \qquad (3)$$

*Work performed under the auspicas of the United States Department of Energy.

†Present address is University of California, Lawrence Berkeley Laboratory, Berkeley, California 94720.

Table I

Triple and Critical Point Properties

Triple Point Properties		CH_4	Ar	Kr	Xe
Temperature,	T_t(K)	90.65	83.806	115.763	161.391
Pressure,	P_t(torr)	87.1	517.1	547.5	612.2
Density					
Gas,	ρ_g(mg/cm³)		4.05	6.52	8.18
Liquid,	ρ_l(gm/cm³)	.405	1.414	2.44	2.96
Solid,	ρ_s(gm/cm³)		1.622	2.79	3.40
Latent heat of vaporation,	L_v(cal/mole)	2033	1579	2191	3048
Latent heat of fusion,	L_f(cal/mole)	224.5	285	392	549
Heat capacity,	C_p(cal/mole K)		10.05	10.7	10.7
Thermal conductivity,	K(cal/sec cm K) x 10^5		29.9	21.1	16.8
Viscosity, bulk;	η_β(millipoise)		1.1	1.9	1.6
shear;	η_s(millipoise)		2.8	4.4	5.2
Critical Point Properties					
Temperature	T_c(K)	190.78	150.70	209.5	289.72
Pressure	P_c(bar)	45.7	48.6	55.2	58.4
Density	ρ_c(gm/cm³)	.160	.53	.918	1.11

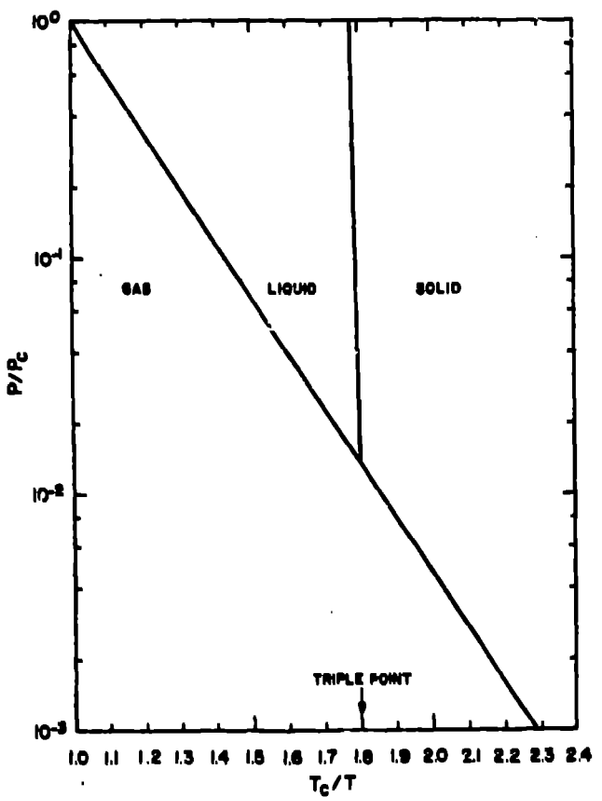

Fig. 1 Phase diagram for rare gas liquids.

A small change in ρ_c for argon and methane yields identical temperature dependences of ρ_l/ρ_c.[9] Note the density is decreasing with temperature (-.86%/K at the triple point of argon) and will change the stopping power by a factor of 2.66 between the triple and critical points.

3. Electrical and Optical Properties

3.1 Electron Transport

Electrons moving in a gas can be viewed as particles moving in a vacuum and occasionally colliding with a gas particle. Electrons moving in a solid must be treated entirely differently. Because of close packing (compared to a gas) and long-range order, interferences of the electron with itself becomes important and electrons are treated as free waves.

Liquids pose a more complicated problem. Over long distances they show gas-like characteristics. They do, however, show short-range order. The structure factor, S(k), function indicates this. Further, the field that an electron sees in a liquid is very different from that of a gas.

Table II

Vaporization and Melting Curve Parameters

Parameter	CH_4	Ar	Kr	Xe
A	5.519	5.332	5.341	5.371
B		3107	3298	3240
C		1.593	1.6169	1.5892
$\left(\frac{dp}{dT}\right)_t$ (bar/K)	32.629	39.2	31.0	25.0

The weakest part of determining the characteris of the electrons in liquids is determining a model for the electron-atom interaction in a liquid. Problems arise because the potential is not a simple two body potential or a sum of two body potentials. This can be explained as follows. Suppose there is an atom at $\vec{R} = 0$ and there is another atom at $\vec{R} = \vec{R}_o$. We want to find the potential the electron sees as a function of r. The electron will induce polarization in each atom. If these polarizations were independent, the resulting field would be the superposition of the two fields. It is clear that the dipoles of the two atoms are not independent, otherwise there would be no liquid state. Further complexity is added to the problem by noting that $\vec{R}_o$ has a statistical distribution of values about several maxima and minima.

There are two approaches that have been used to make the problem tractible. Springett, Jortner, and Cohen used the Wigner-Seitz model.[15] We do not discuss their theory here.

Lekner uses another approach.[16] He approximates the electric field produced by an electron in the liquid as $f(R)\ e/R^2$. Than by looking at a pair of atoms and a self-consistency argument he derives a self-consistency condition for $f(R)$. The resulting $f(R)$ is shown in Fig. 2. He then approximates the exchange and polarization potential by

$$U(R) = -\frac{1}{2}e^2 f(R)/(R^2 + R_\alpha^2)^2 \qquad (4)$$

where R_α is adjusted to fit scattering data. To this he adds the potential from the coulomb field screened by the Hartree distribution of electrons.

$$U_1 = U_H + U_\alpha \qquad (5)$$

He finally points out that the potentials of neighboring atoms overlap so he takes an ensemble average

$$U(R) = U_1(R) + \frac{2\pi}{R}\rho_o \int_o^\infty ds\ sg(s) \int_{|R-s|}^{R+s} dt + U_1(t) \qquad (6)$$

and lets

$$U_{eff} = \langle U(R)\rangle - U_o, \quad R < R_m$$
$$= 0, \quad R > R_m \qquad (7)$$

where R_m is defined by

$$\frac{\partial\langle U\rangle}{\partial R}\Big|_{R_m} = 0, \quad U_o = U(R_m) \qquad (8)$$

All of the appropriate potentials are in Fig. 3.

Once a potential is derived, statistics are used to obtain momentum distribution functions and from that, drift velocities. We consider here a simplified version of the derivation of the drift velocities. There are two pertinent cross-sections in a liquid. They are:

$$\sigma_\varepsilon(\varepsilon) = 2\pi \int_o^\pi d\Theta\ \sin\Theta\ (1 - \cos\Theta)\sigma(\varepsilon,\Theta) \qquad (9)$$

$$\sigma_\varepsilon(\varepsilon) = 2\pi \int_o^\pi d\Theta\ \sin\Theta\ (1 - \cos\Theta)\sigma(\varepsilon,\Theta)\ S(2K \sin\tfrac{\Theta}{2}) \qquad (10)$$

They correspond to the cross section for transferring energy ($\sigma_\varepsilon(\varepsilon)$) and the cross section for transferring momentum ($\sigma_p(\varepsilon)$). Now we assume that all electrons have a mean energy, $\langle\varepsilon\rangle$, and all atoms have an average energy, $\frac{3}{2}kT$. From the conservation of energy we have:

$$\frac{\partial\langle\varepsilon\rangle}{\partial t} = -\delta \frac{m^*}{M^*}\frac{V}{\Lambda_\varepsilon}(\langle\varepsilon\rangle - \tfrac{3}{2}kT) + V_D eE = 0 \qquad (11)$$

From the conservation of momemtum we have:

$$\frac{\partial V_D}{\partial t} = V_D \frac{V\beta}{\Lambda_p} + \frac{eE}{m^*} = 0 \qquad (12)$$

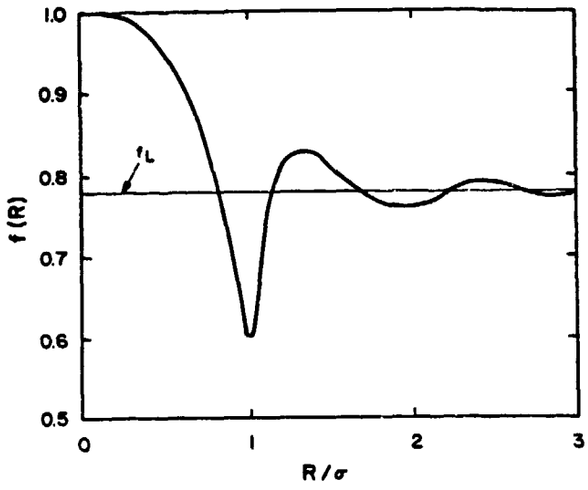

Fig. 2 Local-field function f(R) due to point charge, calculated from the Percus-Yevick pair-correlation function g(R) corresponding to liquid-argon density and a hardcore diameter $\sigma = 3.44$ Å.

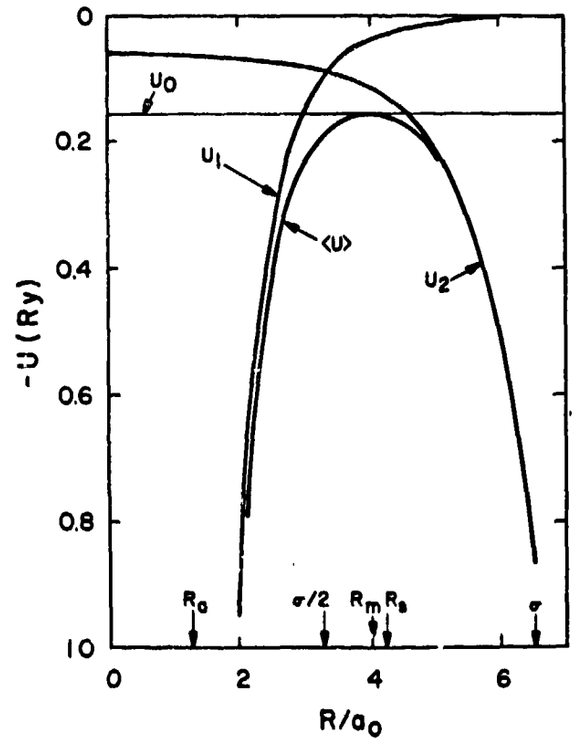

Fig. 3 Atomic potentials in liquid argon. U_0, U_1, <U> are defined in the text.

where m* is the electron effective mass

M* is the atom effective mass

$\Lambda_\varepsilon = (N\sigma_\varepsilon(\langle\varepsilon\rangle))^{-1}$

$\Lambda_p = (N\sigma_p(\langle\varepsilon\rangle))^{-1}$

$\langle\varepsilon\rangle = \frac{m^*V^2}{2}$

Λ_ε is the mean distance to energy transfer

Λ_p is the mean distance to momentum transfer

δ and β are dimensionless variables to account for the statistics. Solving Eqs. 11 and 12 for the mean energy, $\langle\varepsilon\rangle$ and the drift velocity, V_D, we find:

$$\langle\varepsilon\rangle = \frac{3}{4}kT + \left[\frac{9}{16}(kT)^2 + \frac{M^*}{2m^*}\frac{\Lambda_p\Lambda_\varepsilon}{\beta\delta}e^2E^2\right]^{\frac{1}{2}} \qquad (13)$$

$$V_D = \frac{eE\Lambda_p}{(2m^*\langle\varepsilon\rangle)^{\frac{1}{2}}\beta} \qquad (14)$$

We find a good fit to experimental data may be had with $\frac{\partial\beta}{\partial\langle\varepsilon\rangle} \sim \frac{\partial\delta}{\partial\langle\varepsilon\rangle} \sim 0$. Hence the real use of these "constants"is to interpolate between data points. Based on calculations by Yoshino, et al.,[17] Λ_ε can be taken to be constant over large ranges in $\langle\varepsilon\rangle$ and Λ_p ($\langle\varepsilon\rangle$) seems to follow a simple exponential law once it is no longer constant, i.e., for argon $\Lambda_p = 44.3 \times 10^{-8}\langle\varepsilon\rangle^{-.387}$ cm.

In the low field limit, we get the drift velocity introduced by Bardeen and Schockley:[18]

$$V_D = \frac{2}{3}\left(\frac{2}{\pi m^*kT}\right)^{\frac{1}{2}}eE\Lambda_p \qquad (15)$$

A full statistical treatment was given in the calculations of Lekner and Cohen.[19] Lekner[16] and Yoshino, Sowada, and Schmidt[17] use the latter approach in their calculations.

Experiments to measure electron drift velocities in liquid rare gases started in the late forties and continues today. Typical experiments, e.g., Larsh and Davidson,[20] were simple time of flight measurements. Electrons were produced in any number of ways including ionization by alpha particles, field emission tips, direct election injection and ionization from pulsed bremsstahlung from an electron accelerator. Examples of these measurements are Pruett and Broida;[21] Schnyder, Rice, and Meyer;[22] Miller, Howe and Spear;[23] and Yoshino, Sowada, and Schmidt.[17] In the first three cases voltage changes w.r.t. time were usually measured between grids of known spacing. It was assumed that the ionization took place in a close vicinity to its source, and that this distance is small compared to the total drift distance of the electron. In the second case ionization was uniform and the voltage between anode and cathode was monitored as a function of time after the burst of radiation. Data from the measurements is shown in Figs 4-11 (Yoshino, et al.,[17] Sowada, et al.[24]). All of the pure gases show a velocity saturation at very high fields. The saturation velocity, low field mobility and temperature are given in Table III.

Table III

Low-Field Electron Mobility and Saturation Velocity in Liquid CH_4, Ar, Kr, and Xe

Liquid	T(K)	μ_{el} (cm^2V^{-1} sec^{-1})	V_s(cm sec^{-1})	References
CH_4	111	400 ±50		25
Ar	87	400 ±50	6.4×10^5 ±10%	17
	85	520	5	26
	85	475	7.5×10^5	23
	87		6×10^5	21
Kr	120	1200 ±150	4.8×10^5 ±10%	17
	117	1800	3.8×10^5	23
	119		3.3×10^5	21
	120.4	1310		22
Xe	165	2000 ±200	2.6×10^5 ±10%	17
	163	1900	2.9×10^5	23

From Figs. 4-10 it can be seen that small amounts of impurities can greatly change the drift velocity. Swan[27] first noticed this in 1959. This is believed to happen because inelastic scattering of impurity atoms provide a more efficient means of energy loss and hence cool the electrons down. Yoshino, et al.[17] give a simple analysis describing this as follows: The mobility, $\mu(E)$, has its usual definition.

$$\mu(E) = V_D(E)/E \tag{16}$$

If $\mu_i(E_i)$ for an impure substance is the same as $\mu_p(E_p)$ for a pure substance, the mean electron energy is the same for both cases. The additional rate of energy loss because of impurities in solution is:

$$A = (V_{Di}E_i - V_{Dp}E_p)e$$

$$= \mu(E_i^2 - E_p^2)e \tag{17}$$

They define the mean free path between collisions with impurities, Λ_{in}, as:

$$\Lambda_{in} = (N\sigma_{in}(\varepsilon))^{-1} \tag{18}$$

and the average energy loss, ΔW, in inelastic collisions having cross section, $\sigma(\varepsilon)$.

The rate of energy loss, A, is also given by:

$$A = \frac{\Delta W V}{\Lambda_{in}} \tag{19}$$

where $V = (\frac{2\varepsilon}{m^*})^{\frac{1}{2}}$

It is then easily shown that:

$$V_{Di} = [\frac{\mu\Delta W\sigma(\varepsilon)}{e} N(\frac{2\varepsilon}{m^*})^{\frac{1}{2}} + (\mu E_p)^2]^{\frac{1}{2}} \tag{20}$$

Figures 12 and 13 show $\sigma(\varepsilon)\Delta W$ as a function of mean energy, ε, for different impurities.[17] Figure 14 shows $\sigma(\varepsilon)\frac{\Delta W}{\varepsilon}$ as function of the mean energy.[24] It is clear that one wants this product to be as large as possible in order to achieve the fastest charge transport.

3.2 Positive Ion Transports

Very little data exists concerning the positive ion transport in the liquid rare gases. H. Ted Davis, Stuart A. Rice, and Lothar Meyer have measured the mobility of positive ions in liquid argon, krypton, and xenon at various pressures and temperatures.[28] They find that the agreement between experiment and theory is best if they assume the ionic species is Ar_2^+, Kr_2^+, or Xe_2^+ as opposed to a different species such as Ar^+. In Table IV we list the positive ion mobilities determined by Ted Davis, et al. The mobility for positive ions in liquid methane was determined by G. Bakale and W. F. Schmidt.[25]

T. H. Dey and T. J. Lewis[29] measure the mobility of Ar_2^+ at 87 K in liquid argon to be 2×10^{-4} cm^2V^{-1} sec^{-1}. Evidence for a less mobile species of ions (positive?) in liquid rare gases have been eluded too.[30,31] It is highly desirable to have more precise experiments on the positive ion transport.

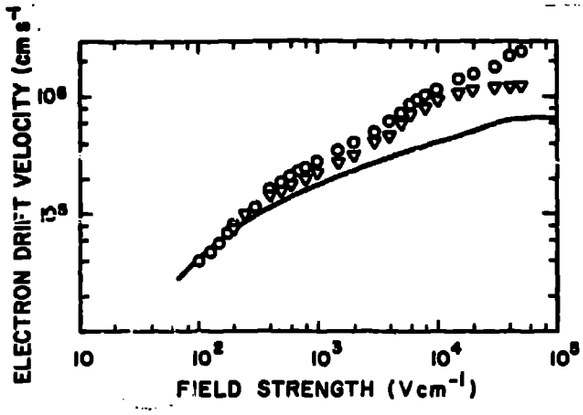

Fig. 4 Influence of methane on the electron drift velocity in liquid argon. ▽: 2.6 x 10^{20} cm^{-3}; ○: 6.5 x 10^{20} cm^{-3}. T(Ar) = 87°K. Solid line: pure argon.

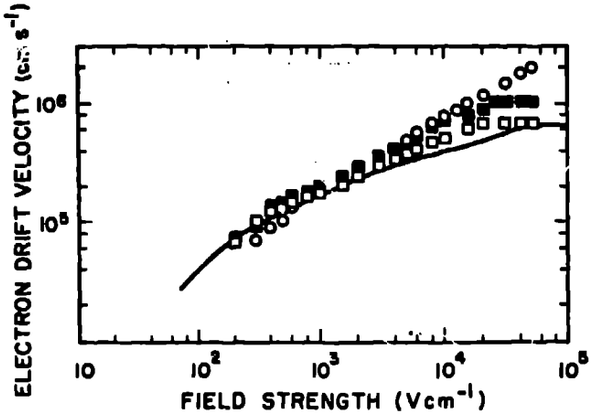

Fig. 5 Influence of propane on the electron drift velocity in liquid argon. □: 2 x 10^{19} cm^{-3}; ■: 7 x 10^{19} cm^{-3}; ○: 4.7 x 10^{20} cm^{-3}; T(Ar) = 87 K. Solid line: pure argon.

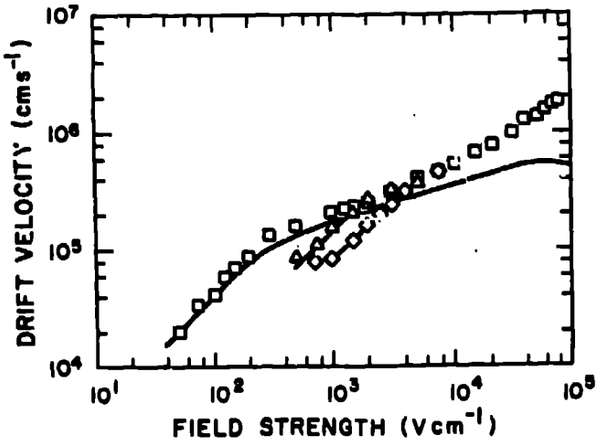

Fig. 6 The influence of carbon monoxide on the electron drift velocity in liquid argon at 87 K. CO concentration: □ 1.7 x 10^{19} cm^{-3}, ◇ 6.5 x 10^{20} cm^{-3}, △ 3.2 x 10^{20} cm^{-3}, — pure argon.

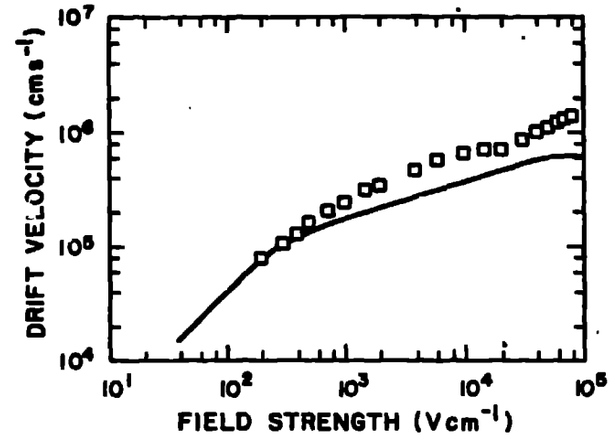

Fig. 7 The influence of propylene on the electron drift velocity in liquid argon. T = 87 K; 1.9 x 10^{19} cm^{-3}.

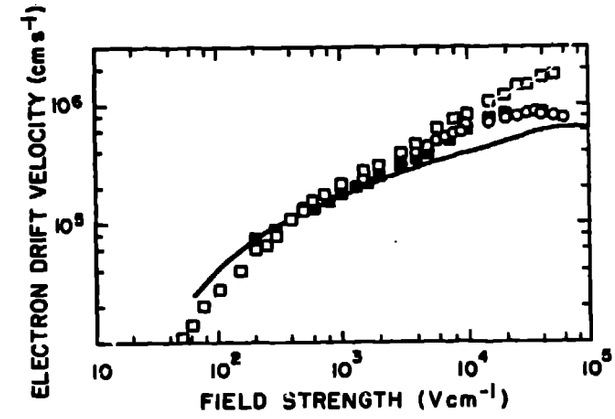

Fig. 8 Influence of ethane on the electron drift velocity in liquid argon. ○: 5.5 x 10^{19} cm^{-3}; ■: 8.7 x 10^{19} cm^{-3}; □: 5 x 10^{20} cm^{-3}. T(Ar) = 87 K. Solid line: pure argon.

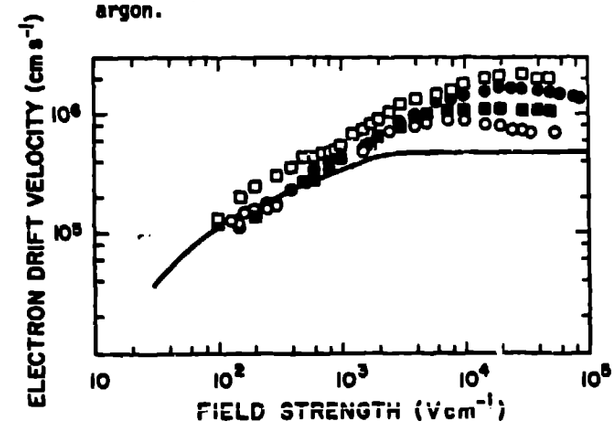

Fig. 9 Influence of methane, ethane, and butane on the electron drift velocity in liquid krypton. Methane: □ ~5 x 10^{20} cm^{-3}; ethane: (○) 2.5 x 10^{19} and (●) 1.2 x 10^{20} cm^{-3}; butane: (■) 4.7 x 10^{19} cm^{-3}. T(Kr) = 120 K. Solid line: pure krypton.

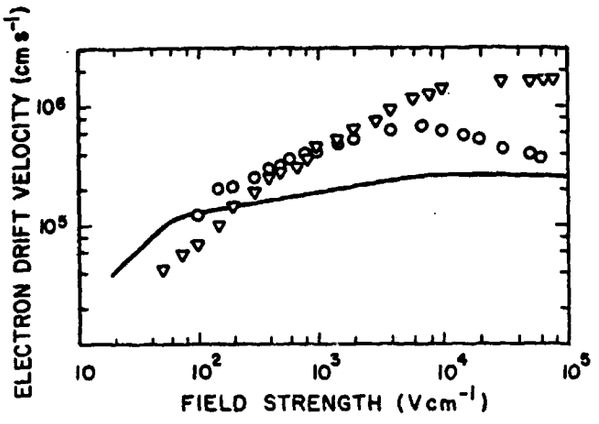

Fig. 10 Influence of butane on the electron drift velocity in liquid xenon. O: 1.26×10^{19} cm^{-3}; ▽: 1.9×10^{20} cm^{-3}. T(Xe) = 165 K. Solid line: pure xenon.

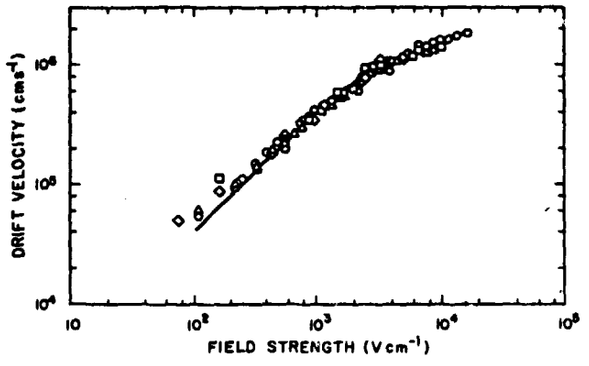

Fig. 11 Dependence of electron drift velocity on electric field strength in liquid methane at T = 111 K, 1 atm □ ○ ▽ ◇ different cells and fillings.

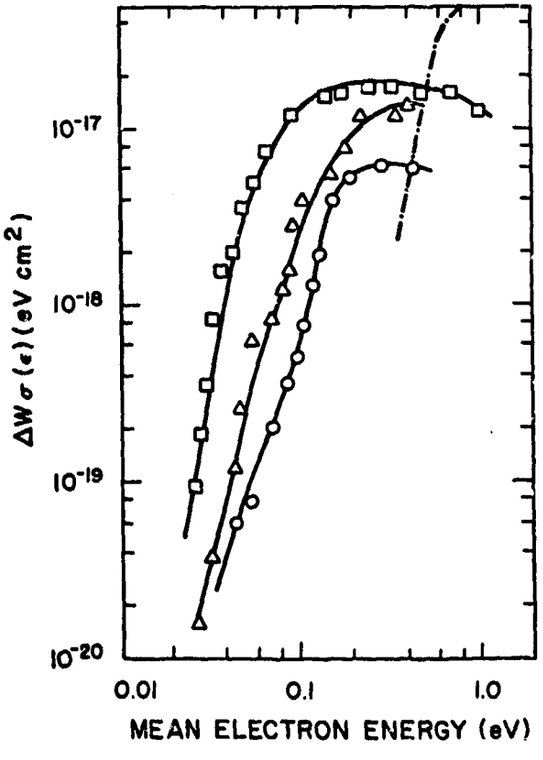

Fig. 12 Product of energy loss quantum ΔW and cross section σ as a function of the mean electron energy ε. O: ethane; Δ: propane; : butane; –·–: hydrogen.

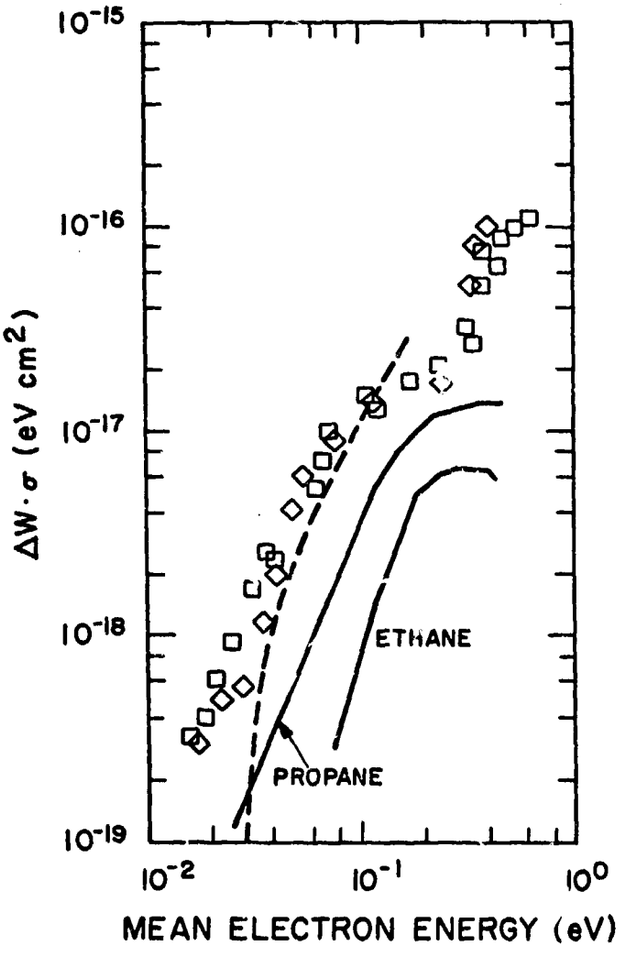

Fig. 13 Product of cross section for energy transfer and energy loss quantum as a function of the electron mean energy: □ : propylene, ◇ ethylene, --- TMS.

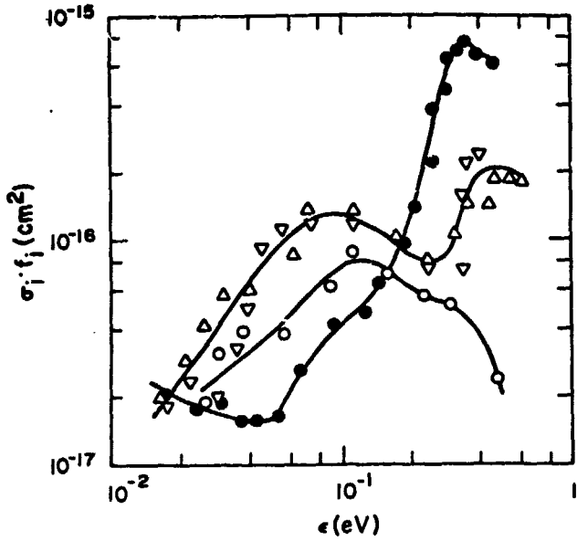

Fig. 14 Product of cross section for energy transfer and the ratio of the inelastic and elastic mean fractional energy losses as a function of the electron mean energy: ○ carbon dioxide, ● carbon monoxide, △ propylene, ▽ ethylene.

Table IV

Positive Ion Mobilities in Liquid Methane, Argon, Krypton, and Xenon

Liquid	T(K)	P(atm)	$\mu \times 10^4$ ($cm^2 V^{-1} sec^{-1}$)
Methane	91	-	16.0
Argon	90.1	5.1	6.12
Krypton	141.0	22.7	6.69
Xenon	184.2	7.5	2.85

3.3 Average Energy Expended per Ion Pair, W

The average energy expended per ion pair in liquids argon, krypton, and xenon have received considerable attention in a sequence of recent publications.[32,36] One of the authors, T. Doke,[27] suggested that the W value in the condensed state of rare gases may have lower value than that in the gaseous state, assuming the presence of a conduction band in the condensed state. This suggestion was verified in subsequent publications.[32,33,35] The measured values of W, the average energy expended per ion pair are listed in Table V. T. Doke, et al.[36] have calculated values of W using an energy balance relation of Platzman[38] and a model of Shockley.[39] The results of these calculations are given in Table V and are seen to be in agreement with the data. T. Doke, et al.[35] also have calculated the Fano-factors, F, for the rare gas liquids, which are given in Table V. It is noteworthy that the predicted statistical limited energy resolution for liquid xenon is only two times that of germanium.

S Kubota, et al.[34] have observed an enhanced ionization yield (13% relative to the ionization yield in pure liquid argon) for Xe-doped (1.6%) liquid Ar. They attribute this enhancement to the ionizing excitation transfer process from Ar excitons to doped Xe. The equivalent enhancement in ionization yield with Kr-doped liquid argon was not observed. Doke, et al.[36] estimate the Fano-factor for xenon-doped (1.6%) liquid argon for Shockley's model to be F = 0.064.

The recent results of Huang and Freeman[40] on the energy expended per ion pair are not given here because of the unresolved question of the voltage dependence in their W values.

4. Effect of Impurities

4.1 Effect of Impurities on Charge Transport

In Section 3.1 we showed how impurities through inelastic collisions could speed up the electron transport. If the impurity-electron interaction is such that the impurity captures the electron (electron attachment or scavenging), the mobility is reduced by many orders of magnitude. The subject of electron scavenging is reviewed extensively by Hummel.[3] The electron attachment rates have been recently measured for O_2 and N_2 by W. Hofmann, et al.[41] and for SF_6, N_2O, and O_2 in liquid argon and xenon by Bakale, Sowada, and Schmidt.[42] This latter paper discusses the smallness of the attachment cross section with O_2 relative to the other impurities and and a maximum attachment cross section[43] given by:

$$\sigma_{max}(V) = \pi\lambda^2 \qquad (21)$$

with $\lambda = 2\pi\lambda$ the de Broglie wave length of the electron. The energy dependence of σ_{max} is:

$$\sigma_{max}(\epsilon) = \frac{h^2}{8\pi m\epsilon} = \frac{1.2 \times 10^{-15}\ cm^2}{\epsilon(eV)} \qquad (22)$$

Table V

Average Energy Expended per Ion Pair

Liquid	E_{gap} (eV)	$W_{exp.}$ (eV/Ion Pair)	W_{theory} (eV/Ion Pair)	F_{theory}
Argon	14.3	23.6 ±0.3	23.3	0.107
Krypton	11.7	20.5 ±1.5	19.5	0.057
Xenon	9.28	15.6 ±0.3	15.4	0.041

The attachment cross-section measured for O_2 is three orders of magnitude smaller than given by $\sigma_{max}(\varepsilon)$. This emphasizes the importance of impurities other than O_2 in the rare gas liquids and is discussed further in a recent paper of Gruhn and Maier.[44] The mobility of these negative ions is similar to that of the positive ions (10^{-4} $cm^2V^{-1}sec^{-1}$).

4.2 Solubility of Impurities in Liquid Methane, Argon, Krypton, and Xenon

Little experimental information is available on the solubility of solids in the rare gas liquids and liquid methane. The solubilities of hydrocarbons and carbon dioxide in liquid methane and liquid argon have been reported recently.[45,46] They report the mole fraction, X, of impurities saturated in solution as a function of temperature.

4.3 Impurity Monitor

In a recent paper Gruhn and Maier, II[44] demonstrate the utility of infrared absorption spectroscopy as a means of monitoring impurities in liquid ion chamber media. They demonstrate sensitivities to low concentrations (ppm-ppb) dependent upon the infrared absorption cross section.

In Fig. 15 we show the infrared absorption spectrum through one meter of spectral grade (99.995%) liquid xenon. The CO_2 concentration is estimated to be about 50 ppb. The features that appear near 1250 cm^{-1} are tentatively assigned to a C-F stretching vibration and probably arise from halocarbon compounds having concentrations of a few parts per million.

It was noted that the halocarbon concentrations vary from cylinder to cylinder of gas and even more drastically between manufacturers.

Figure 16 shows the effect of flow rate on the removal by a hydrox purifier on impurities in spectral grade xenon. Notice that the zero and 100% lines for each curve have been displaced by the same amount of the ordinate for better display. Curve a is the absorption spectrum of unpurified liquid zenon. Curve b is the spectrum of the liquid condensed from gas flowed through the purifier at 2 l/min. Curve c is the spectrum of the liquid condensed from gas flowed through the purifier at 0.2 l/min. The small features between 2800 and 3000 cm^{-1} are due to a material absorbed on the windows. The CO_2 concentration in curve a is about 3 ppm. The feature that appear near 1250 cm^{-1} in curve a are tentatively assigned to a C-F stretching vibration and probably arise from halocarbon compounds having concentrations of a few parts per million. It is observed in Fig. 16 that the efficiency of the hydrox purifier is both flow rate and impurity dependent.

5. Atomic and Nuclear Properties

The atomic and nuclear properties have been tabulated by the LBL nuclear particle data group.[47] In Table VI we list these properties for liquid methane, argon, krypton, and xenon. We have interpolated the values of the nuclear cross sections, specific energy loss, and radiation lengths for krypton and xenon from the data in Reference 47. Methane was assumed to have the same values as propane for these properties.

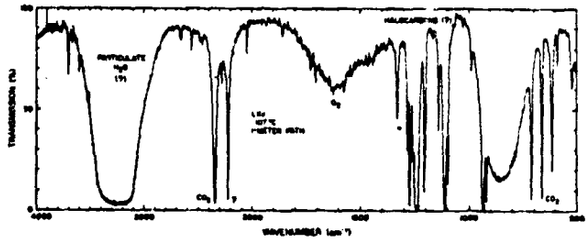

Fig. 15 Infrared absorption spectrum through one meter of spectral grade (99.995%) liquid xenon.

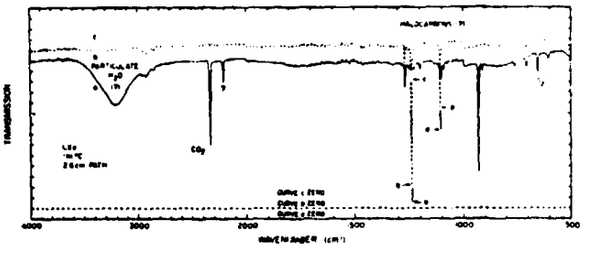

Fig. 16 Effect of flow rate through a hydrox purifier on the removal of impurities in xenon. The instrumental resolution is ~4 cm^{-1}.

Table VI

Atomic and Nuclear Properties

Property	CH_4	Ar	Kr	Xe
Z		18	36	54
A	16.043	39.944	83.80	131.3
Nuclear cross section [barns]		.890	1.56	2.15
Nuclear collision length [g/cm^2]	55.0	78.8	89.5	101.8
[cm]	134	53.0	36.7	34.4
Absorption length λ [cm]	176	80.9		
dE/dX min MeV/g/cm^2	2.28	1.51	1.30	1.25
MeV/cm	.98	2.11	3.17	3.70
Radiation length, L_{rad} [g/cm^2]	44.7	19.6	11.2	8.4
[cm]	110.4	13.9	4.59	2.84
Density at triple point [g/cm^3]	.405	1.41	2.44	2.96
Refractive index, N	1.25	1.25	1.33	1.41
Gas/liquid vol. ratio		784.0	643.6	518.9

Acknowledgments

The authors gratefully acknowledge the aid of Maudie Noyd of Lawrence Berkeley Laboratory, California, in the preparation of this manuscript.

References

1. R. K. Crawford, edited by M. L. Klein and J. A. Venables, Rare Gas Solids, London: Academic Press, 1977, Vol. II, p. 663.
2. A. C. Hollis Hallett, edited by G. A. Cook, Argon, Helium and the Rare Gases, New York/ London: Interscience Publishers, Inc., 1961, Vol. I, p. 313.
3. A. Hummel, Advances in Radiation Chemistry, New York: Wiley-Interscience, 1974, Vol. IV, p. 1.
4. A. Mozumder, Advances in Radiation Chemistry, New York: Wiley-Interscience, 1969, Vol. II, p. 1.
5. J. De Boer and A. Michels, Physica 5, 1938, 945.
6. K. S. Pitzer, Journal Chem. Physics 7, 1939, 583.
7. E. A. Guggenheim, Journal Chem. Physics 13, 1945, 253.
8. W. B. Streett and L.A.K. Staveley, Physica 71, 1974, 51.
9. M. J. Terry, T. J. Lynch, M. Bunclark, K. R. Mansell, and L.A.K. Staveley, Journal Chem. Thermodynamics 1, 1969, 413.
10. T. R. Strobridge, U.S. Natl. Bur. Std., Tech. Note 129, 1962.
11. W. B. Streett, Physica 76, 1974, 59.
12. W. B. Streett, L. S. Sagan, and L.A.K. Straveley, Journal Chem. Thermodynamics 5, 1975, 633.
13. F. E. Simmon and G. Glatzel, Z. Anorg. U. Allgem. Chem. 78, 1929, 309.
14. S. E. Babb, Jr., Rev. Mod. Phys. 35, 1963, 400.
15. B. E. Springett, J. Jortner, and M. H. Cohen, Journal Chem. Phys. 48, 1968, 2720.
16. J. Lekner, Phys. Rev. 158, 1967, 130.
17. K. Yoshino, U. Sowada, and W. F. Schmidt, Phys. Rev. A14, 1976, 14.
18. J. Bardeen and W. Schockley, Phys. Rev. 80, 1950, 72.
19. M. H. Cohen and J. Lekner, Phys. Rev. 158, 1967, 305.
20. N. Davidson and A. E. Larsh, Jr., Phys. Rev. 77, 1950, 706.
21. H. D. Pruett and H. P. Broida, Phys. Rev. 169, 1967, 1138.
22. H. Schnyders, S. A. Rice, and L. Meyer, Phys. Rev. 150, 1966, 127.
23. L. S. Miller, S. Howe, and W. E. Spear, Phys. Rev. 166, 1968, 871.
24. U. Sowada, W. F. Schmidt, and G. Bakale, Can. Journal Chem. 55, 1977, 1885.
25. G. Bakale and W. F. Schmidt, Z. Naturforsch, 28a 1973, 511.
26. B. Halpern, J. Lekner, S. A. Rice, and R. Gomer, Phys. Rev. 156 1967, 351.
27. D. W. Swan, Proc. Phys. Soc. 83, 1964, 659.
28. H. T. Davis, S. A. Rice, and L. Meyer, Journal Chem. Phys. 37, 1962, 947.
29. T. H. Dey and T. J. Lewis, Brit. Journal Appl. Phys. Ser. 21, 1968, 1019.
30. C. R. Gruhn and M. D. Edmiston, Phys. Rev. Lett. 40, 1978, 407.
31. I. Roberts and E. G. Wilson, Journal Phys. Chem. 6, 1973, 2169.
32. M. Miyajima, T. Takahashi, S. Konno, T. Hamada, S. Kubota, E. Shibamura, and T. Doke, Phys. Rev. A9, 1974, 1438, and Phys. Rev. A10, 1974, 1452.
33. T. Takahashi, S. Konno, T. Hamada, M. Miyajima, S. Kubota, A. Nakamoto, A. Hitachi, E. Shibamura, and T. Doke, Phys. Rev. A12, 1975, 1771.
34. S. Kubota, A. Nakamoto, T. Takahashi, S. Konno, T. Hamada, M. Miyajima, A. Hitachi, E. Shibamura, and T. Doke, Phys. Rev. B13, 1976, 1649.
35. T. Takahashi, S. Konno, and T. Doke, Journal Phys. C7, 1974, 230.
36. T. Doke, A. Hitachi, S. Kubota, A. Nakamoto, and T. Takahashi, Nucl. Instr. and Meth. 134, 1976, 353.
37. T. Doke, Butsari: Monthly Review Journal published by Phys. Soc. Japan 24, 1969, 609.
38. R. L. Platzman, Int. Journal Appl. Rad. Isotopes 10, 1961, 116.
39. W. S. Shockley, Czech. Journal Phys. B11, 1961, 81.
40. S.S.S. Huang and G. R. Freeman, Can. Journal Chem. 55, 1977, 1838.
41. W. Hofmann, U. Klein, M. Schulz, J. Spengler, and D. Wegener, Nucl. Instr. and Meth. 135, 1976, 151.
42. G. Bakale, U. Sowada, and W. F. Schmidt, Journal Phys. Chem. 80, 1976, 2556.
43. L. G. Christophorou, D. S. McCorkle, and J. C. Carter, Journal Chem. Phys. 54, 1971, 253.
44. C. R. Gruhn and W. B. Maier, II, submitted to Nucl. Instr. and Meth. 1978.
45. G. T. Preston, E. W. Funk, and J. M. Prausnitz, Journal Phys. Chem. 75, 1971, 2345.
46. A. de Mateo and F. Kurata, Ind. Eng. Chem., Process Des. Dev. 14, 1975, 137.
47. Particle Data Group, Rev. Mod. Phys. 48, 1976, S1.